WIMP-nucleon cross-section results
from the second science run of ZEPLIN-III

D.Yu. Akimov[a], H.M. Araújo[b,*], E.J. Barnes[c], V.A. Belov[a], A. Bewick[b], A.A. Burenkov[a], V. Chepel[d], A. Currie[b], L. DeViveiros[d], B. Edwards[e], C. Ghag[c], A. Hollingsworth[c], M. Horn[b], W.G. Jones[b], G.E. Kalmus[e], A.S. Kobyakin[a], A.G. Kovalenko[a], V.N. Lebedenko[b], A. Lindote[d,e], M.I. Lopes[d], R. Lüscher[e], P. Majewski[e], A.St J. Murphy[c], F. Neves[d,b], S.M. Paling[e], J. Pinto da Cunha[d], R. Preece[e], J.J. Quenby[b], L. Reichhart[c], P.R. Scovell[c], C. Silva[d], V.N. Solovov[d], N.J.T. Smith[e], V.N. Stekhanov[a], T.J. Sumner[b], C. Thorne[b], R.J. Walker[b]

[a]*Institute for Theoretical and Experimental Physics, Moscow, Russia*
[b]*High Energy Physics group, Blackett Laboratory, Imperial College London, UK*
[c]*School of Physics & Astronomy, SUPA University of Edinburgh, UK*
[d]*LIP–Coimbra & Department of Physics of the University of Coimbra, Portugal*
[e]*Particle Physics Department, STFC Rutherford Appleton Laboratory, Chilton, UK*

Abstract

We report experimental upper limits on WIMP-nucleon elastic scattering cross sections from the second science run of ZEPLIN-III at the Boulby Underground Laboratory. A raw fiducial exposure of 1,344 kg·days was accrued over 319 days of continuous operation between June 2010 and May 2011. A total of eight events was observed in the signal acceptance region in the nuclear recoil energy range 7–29 keV, which is compatible with background expectations. This allows the exclusion of the scalar cross-section above 4.8×10^{-8} pb near 50 GeV/c^2 WIMP mass with 90% confidence. Combined with data from the first run, this result improves to 3.9×10^{-8} pb. The corresponding WIMP-neutron spin-dependent cross-section limit is 8.0×10^{-3} pb. The ZEPLIN programme reaches thus its conclusion at Boulby, having deployed and exploited successfully three liquid xenon experiments of increasing reach.

Keywords: ZEPLIN-III, dark matter, WIMPs, liquid xenon detectors

1. Introduction

Direct, indirect and accelerator searches for neutralino dark matter are now probing regions of parameter space favoured by minimal supersymmetric (SUSY) extensions to the standard model, in particular those constrained at the unification scale and by measurements of cosmological cold dark matter abundance. SUSY is motivated by the need to stabilise the weak scale, but it is remarkably persuasive that *R*-parity conserving flavours of the theory lead to an excellent WIMP dark matter candidate in the form of the lightest SUSY particle. However, at a time when no evidence for SUSY has yet emerged at the LHC [1, 2, 3, 4, 5], it is worth noting that direct searches, such as the one reported here, aim to detect any WIMP, not just neutralinos. Such experiments exploit the possibility that WIMPs may scatter off ordinary baryonic matter. The experimental challenge lies in conducting a rare event search ($\lesssim 1$ evt/kg/yr) whilst maintaining efficient detection of very low energy signatures (few keV). Liquid xenon (LXe) is an excellent target material for intermediate mass WIMPs due to its high atomic mass and sensitivity in two response channels (scintillation and ionisation).

Significantly, these allow discrimination between electron recoils resulting from radioactivity backgrounds and the nuclear recoils expected from WIMP elastic scattering.

The ZEPLIN-III experiment operated at the Boulby laboratory (UK) under a rock overburden of 2,850 m water equivalent. This two-phase xenon emission detector measures both scintillation and ionisation responses from particle interactions in its 12-kg LXe target. Approximately half of this mass forms a 'fiducial' region with well understood performance and backgrounds. The ionisation released at an interaction site is drifted upward and emitted into a thin (few mm) vapour phase above the liquid, where it is converted into an optical signal via electroluminescence. This is achieved with a strong electric field of 3–4 kV/cm in the liquid phase (approximately twice as strong in the gas). An array of 31 photomultiplier tubes (PMTs) is located within the cold liquid and views the 36.5-mm thick active region above it. The array responds to the prompt scintillation and the delayed electroluminescence signals (termed S1 and S2, respectively). A detailed description of the detector design and construction can be found in Refs. [6, 7]. This time projection chamber configuration allows very good position reconstruction in three dimensions, as well as electron/nuclear recoil discrimination which is critical for WIMP searches [8, 9, 10].

The first science run (FSR) of the experiment in 2008 placed very competitive upper limits on the WIMP-nucleon scattering cross sections in several interaction models [11, 12, 13]. The FSR sensitivity was limited by background originating from PMT γ-rays. In particular, the most challenging event topology in ZEPLIN-III comes from multiple-scintillation single-ionisation (MSSI) events, whereby a single interaction vertex in the active region (producing both S1 and S2) is accompanied by one or more scatters in a region yielding no charge (S1 only). As the scintillation responses are effectively time-coincident, S2/S1 ratios reconstructed for these γ-ray events are essentially lower than typical for single-scatter electron recoils, and they can leak down to the nuclear recoil acceptance region. Nevertheless, we were able to achieve an average electron/nuclear recoil discrimination power of 7,800:1 in the 2–16 keVee WIMP search region, which is the best reported for a LXe detector (hereafter, 'keVee' represents the electron-equivalent energy as calibrated by 122 keV ^{57}Co γ-rays and 'keVr' denotes nuclear recoil energy).

Two upgrades of the experiment had been planned from its inception. The first was the replacement of the PMT array, which dominated the γ-ray and neutron background budgets in the FSR by a large factor. A new PMT model (ETEL D766Q [14]) was developed in collaboration with the manufacturers, which delivered a 40-fold improvement in γ-ray activity per unit. This allowed an 18-fold reduction in overall electron recoil background at low energies relative to the FSR. In Ref. [15] we analysed the radioactivity backgrounds affecting the experiment in the second run and showed that they were predicted with good precision. Unfortunately, the optical and electrical performances of the new PMTs were substantially poorer than those of the previous tubes; worse still, the dispersion of gains and quantum efficiencies (QE) posed very considerable problems to data analysis. Obtaining a set of working PMTs and coping with this variability across the array became the main challenge of the second run.

The second major upgrade was the addition of an anti-coincidence veto system, which was retrofitted around the ZEPLIN-III target [16, 17]. This 52-module plastic scintillator detector envelops a Gd-loaded polypropylene shield ($\approx 3\pi$ coverage) which provides moderation and radiative capture of internal neutrons; the mean capture time is 10.7±0.5 μs. The assembly fits inside the lead shield used in the FSR. The veto provides 60% tagging efficiency for internal neutrons, mostly derived from a 0.2–70 μs delayed coincidence window from the ZEPLIN-III trigger point (58%); elastic recoils in the plastic scintillator within a narrow prompt window (±0.2 μs) make up the remaining neutron efficiency. The tagging efficiency for γ-rays in the prompt window was 28%. Adding to its background rejection capability, this tonne-scale detector provides a useful source of diagnostic for the radiation environment around the instrument.

Minor upgrades were also implemented to aid with calibration of ZEPLIN-III. The radioactive source delivery system was fully automated. A copper structure ('phantom' grid) was installed above the anode mirror; this cast a shadow from ^{57}Co γ-rays onto the LXe surface, thus providing calibration of the position reconstruction algorithm. A new fibre-coupled LED light gun helped with calibration of the PMT single photoelectron responses. All of the above upgrades were manufactured from low background components.

2. Second science run

In the second science run (SSR), WIMP-search data were acquired over 319 days between 24th Jun 2010 and 7th May 2011, giving a fiducial exposure of 1,344 kg·days. A 20% reduction from the FSR fiducial mass to 5.1 kg was motivated by the poor performance of peripheral PMTs. Even so, the SSR accumulated 3 times more exposure, and achieved the longest continuous WIMP run of a xenon detector to date. A daily operational duty cycle of 96% was achieved consistently, with 1 hr per day reserved for ^{57}Co calibration and cryogen re-filling; these tasks were automated and controlled remotely. On a weekly basis, the system levelling was adjusted (to compensate for local geological movement) and the target and veto PMTs were calibrated with their respective fibre-coupled LED systems. The gas phase was ∼3.5 mm thick and kept at 1.6 bar, with 13 mbar rms variability within the dataset. The electric field in the liquid was 3.4 kV/cm. A free electron lifetime of 14 μs was achieved by prior purification with a hot getter (comparable to the 13-μs drift time for the deepest fiducial interactions). As observed in the FSR, the lifetime increased steadily without external purification during the run, and eventually reached ∼45 μs.

Data acquisition procedures were described with the FSR results [11] and we provide only a brief summary here. The ZEPLIN-III trigger is derived from the 31-PMT sum signal; the SSR hardware threshold corresponded to the electroluminescence of ≈5 electrons; this translates to ≈10 ionisation electrons in the liquid (average over fiducial interactions in the dataset) when the finite electron lifetime and 66% emission probability at the surface are accounted for. Single emitted electrons generate a mean response of 11.8±0.4 photoelectrons (phe); a study of the single electron signature can be found in Ref. [18]. This S2-derived signal also triggers the veto data acquisition. The two data streams are recorded and reduced separately, and synchronised offline. The ZEPLIN-III waveforms are digitised at 500 MS/s for ±18 μs around the trigger point. Key detector and environmental data from the 'slow control' acquisition system were embedded into the main data.

2.1. Data analysis

Pulse-finding and parametrisation of the waveforms were carried out by ZE3RA [19], our event reduction software. The reduced data were then searched for single scatter events (single S1 and S2 pulses) which were retained for

further analysis. Several corrections were applied, mainly to the S2 response, based either on the slow-control information embedded with each event, or on historical trends derived from the daily calibration. The mean electron lifetime correction was 37%, averaged over the fiducial dataset; also corrected were the electronics gain drift (4.7% rms), detector tilt (1.9%) and pressure variations (1.1%).

A vertex reconstruction algorithm estimated the energy (E) and position (x,y) of the interactions, with a maximum likelihood fit to the S1 response and a least squares fit to the S2 channel [20]. The algorithm fits to 31 empirical response functions simultaneously. These model the response of a PMT as a function of distance to its axis, and are derived from calibration data in an iterative procedure which also 'flat-fields' the array. The spatial resolution thus achieved was 13 mm in S1 and 1.1 mm in S2 (FWHM). The (E,x,y) parameter space was navigated with a *simplex* method to obtain the best fit point for each event; spatial maps of likelihood and χ^2 could also be produced to help identify multiple vertices.

Finally, fiducialisation and quality cuts were applied to the data. A central region of 140 mm radius containing 5.1 kg of LXe was retained. The quality cuts eliminate likely MSSI events and outliers in several parameters (e.g. goodness-of-fit of S1 and S2 reconstructions). An S1 pulse timing cut was also used to exploit modest pulse shape discrimination at the higher energies. The inefficiencies incurred from these cuts are described in the next section. Unsurprisingly, they are more severe than had been required for FSR data.

A blind analysis was conducted during the initial optimisation of the quality cuts and definition of the WIMP acceptance region: low energy events in and around the signal region were kept hidden from visualisation and reduction using a 'blindness manager' implemented in ZE3RA. Vetoed events (mostly γ-rays) were excluded from this list, thus providing a (practically) signal-free population of background events. This blind analysis was not pursued to its ultimate conclusion but the acceptance region (which had been defined blindly) was retained in order to avoid major bias in estimating a potential signal.

2.2. Calibration and efficiencies

Daily calibration with ^{57}Co γ-rays (mostly 122 keV) defined the S1 and S2 energy scales and monitored their stability throughout the run; it also provided a regular measurement of the detector tilt (through the spatial dependence of the S2 pulse width) and of the free electron lifetime (by S2/S1 ratio with interaction depth). The latter parameter was confirmed independently with a new method based on single electron counting operating on the actual science data waveforms [18].

In the SSR the light yield of the chamber (fiducial average) was 1.3 phe/keVee, down from 1.8 phe/keVee in the FSR. The energy resolution was similarly affected; a linear combination of S1 and S2 responses which exploits their microscopic anti-correlation yielded 16.4% (FWHM) for
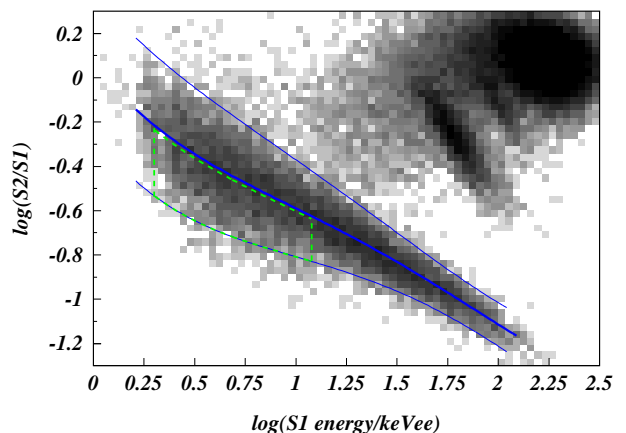

Figure 1: Discrimination parameter as a function of S1-derived energy for Am-Be neutron calibration. The recoil population median and ±2-σ lines are shown (in blue), along with the 2–12 keVee search box (dashed green).

the new array, against a very impressive 8.4% achieved for FSR data using the same analysis codes. In spite of this, a spatial resolution of 1.1 mm (FWHM) in the horizontal plane was achieved in the SSR, measured from the shadow pattern cast by the new phantom grid for ^{57}Co γ-rays.

The electron-recoil population was calibrated with a 4.6 kBq ^{137}Cs source located above the instrument, producing a rate of 150 c/s in the detector. The number of low-energy events thus obtained was similar to that of background electron recoils in the search data.

Three neutron calibrations took place during SSR datataking, totalling 10 hours of exposure to an Am-Be (α,n) source emitting 1,321$\pm$14 n/s [21]; absolute differential rates of nuclear recoils from elastic scatters agreed within statistical errors for these datasets. The delayed-coincidence veto efficiency for such events was 58% independently of recoil energy [17] (the delayed detection is provided by ^{158}Gd γ-rays rather than by the neutrons directly). One such run is depicted in Figure 1. The recoil band populated by neutron elastic scattering was parametrised by Gaussian fitting to the discrimination parameter $\log_{10}$(S2/S1) in 1 keVee (S1) bins. Energy-dependent mean (μ) and width (σ) parameters were used to define a signal acceptance region in the range 2–12 keVee and including approximately the lower half of signal acceptance as indicated in the same figure: from 2.3% ($\mu - 2\sigma$) to 45% ($\mu - 0.126\sigma$). This region was defined before the data within it were revealed.

New measurements of the relative scintillation efficiency for nuclear recoils in LXe (L_{eff}) were derived from FSR and SSR calibration data [22]. The decreasing L_{eff} curves obtained therein were mutually consistent and agree, within experimental errors, with recent neutron beam data [23, 24]. For the purpose of converting between electron and nuclear recoil energies we combined the two ZEPLIN-III measurements into the curve shown in Fig-
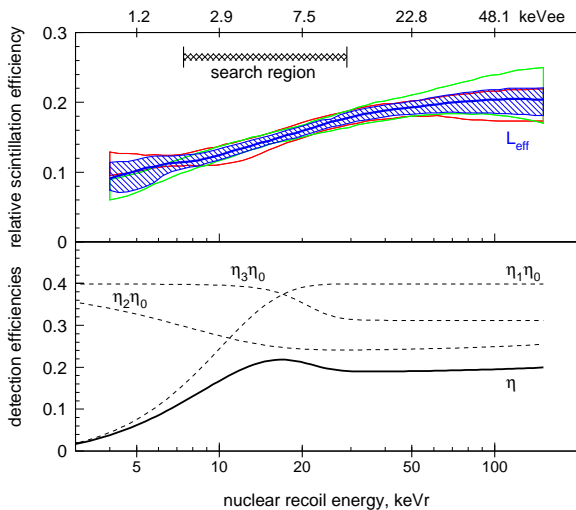
Figure 2: Nuclear recoil efficiencies. Above: relative scintillation efficiency for nuclear recoils in LXe at zero electric field; the thick blue curve (adopted) combines the measurements and uncertainties reported in Ref. [22] for FSR data (68% confidence region, in red) and SSR data (green). Below: recoil detection efficiencies; η subsumes a flat component η_0=39.8% (dominated by signal acceptance in S2/S1) and three energy-dependent factors: η_1 is the S1 detection efficiency from the 3-fold PMT coincidence required in software; η_2 is incurred from quality cuts; η_3 relates to the timing cut on S1 pulses.

ure 2 (upper panel). The SSR WIMP search region corresponds to 7.4–29 keVr.

The nuclear recoil detection efficiency comprises several components. A set of constant factors combine to η_0=39.8%, including: DAQ livetime fraction (99.2%), waveform quality cuts (98.3%), pulse parameter cuts (96.9%), veto random coincidences (99.6% and 99.0% for the prompt and delayed windows, respectively) and the above signal acceptance fraction (42.7%). Three additional curves, shown in Figure 2 (lower panel), describe the detection efficiency for S1 pulses (3-fold requirement in software), the efficiency of the data quality cuts and the additional timing cut on S1 signals for pulse shape discrimination. The effective exposure for a 50 GeV/c^2 WIMP was 251 kg·days.

2.3. Experiment backgrounds

Nuclear recoils from neutron single elastic scattering pose an irreducible background to direct WIMP searches. In ZEPLIN-III, detected radioactivity neutrons are most likely to arise in the ceramic feedthroughs, the PMTs and the laboratory rock; muon-induced neutrons contribute negligibly. The overall predicted rate is 3.05±0.5 events/year in 5–50 keVr assuming unity detection efficiency, as detailed in Ref. [15]. Translated to the SSR effective exposure and search region this gives only 0.06±0.01 events in anti-coincidence with the veto.

A low-energy electron recoil background rate of 0.75 evts/kg/day/keVee ('dru') was measured in the fidu-

cial volume (with no quality cuts applied), which represents a 20-fold reduction brought about by the new phototubes. Monte Carlo predictions from a comprehensive inventory of background sources, based on component-level radio-assays, indicated 0.86±0.05 dru [15]. Background electron recoils are promptly tagged in the external veto with 28% efficiency below ~100 keVee. This confirms that internal β^- emitters are insignificant, since the veto efficiency for coincident γ-rays is practically identical to this value. Independently, we measured the ^{85}Kr decay rate at 7±2 mdru [15].

Assuming the discrimination factor achieved in the first run, electron-recoil event leakage into the WIMP acceptance region should represent <1 event, in line with the aspiration of a background-free second run which motivated the experiment upgrades. However, analysis of the prompt-vetoed γ-rays revealed that this was unlikely to be the case. Background predictions (discussed below) based on extrapolation of the electron recoil population into the signal box and from low-energy ^{137}Cs data indicated that a handful of unvetoed events (7–9) were expected, confirming a loss of discrimination power.

3. WIMP-search results

Upon unblinding, 12 events were observed in the acceptance region. A detailed waveform inspection revealed larger than expected cross-talk artifacts due to the poor electrical performance of the SSR PMTs: gains differed by as much as 100 times within the array, and the extra amplification required in some channels exposed contamination from the higher gain channels (the array is powered by a single HV supply using common dynode electrodes internally). Tighter cuts were required to deal with this issue (Figure 2 already reflects this). The result of the final (non-blind) analysis is shown in Figure 3. Eight events remained in the box. The event reconstructed at 3.2 keVee in S1 and 1.1 keVee in S2 appears far below the mean $\log_{10}$(S2/S1) for typical electron recoils with that S1 energy, but this is not necessarily anomalous: given 1.3 phe/keVee scintillation yield, Poisson fluctuations for events with 1.1 keVee expectation in S1 give 5% probability of generating ≥4 phe, thereby producing the observed S2/S1 ratio or lower.

No *delayed* coincidences were recorded below the nuclear recoil median and those registered above it are statistically consistent with random coincidences. This allows us to set an upper limit of 0.75 neutron events for the search region (90% CL), confirming the successful mitigation of the neutron background. Two methods were used to predict counts from electron recoil backgrounds; both are in good agreement with the observation, suggesting no significant signal. Binned Skew-Gaussian (SG) fits to the $\log_{10}$(S2/S1) parameter above the search region, as in the FSR analysis [11], predict a total of 6.5±3.4 events (cf. 8 observed). ^{137}Cs calibration data provided independent confirmation of this background within the available

Table 1: Observations (n_{obs}), background estimates ($\mu_{b1,2}$) and limits on the signal expectation (μ_s) for the first (FSR) and second (SSR) runs of ZEPLIN-III. Fiducial and net effective exposures (50 GeV/c^2 WIMP) are presented along with relevant signal acceptance parameters. Electron recoil background expectations are estimated from Skew-Gaussian (SG) fits to data above the search region in 2 keVee bins and also from ^{137}Cs calibration. The 90% CL limit on the number of signal events in each run is derived with the Profile Likelihood Ratio method.

run	kg·days (net)	acceptance keVr	fraction	n_{obs}	neutrons μ_{b1}	electron recoils, μ_{b2} SG fit	Cs-137	μ_s 90% CL
FSR	437.0	7–35	29–50%	4	0.5±0.3	5.2±3.1	–	<4.2
	(107.3)		2–29%	1	0.7±0.3	1.5±1.7	–	
SSR	1,343.8	7–29	24–45%	7	0.03±0.005	5.5±2.2	8.3±2.9	<5.1
	(251.0)		2–24%	1	0.03±0.005	1.0±1.2	1.0±1.0	

accuracy, with no contamination from signal and no assumption of a functional dependence for electron recoils; this yielded 9 events for 96% equivalent exposure.

To account for the non-uniform background in $\log_{10}$(S2/S1) we partitioned the search region in two; this was done explicitly to maximise sensitivity given the SG background distributions. Note that the contents of the search region were *not* considered in this optimisation. To achieve this the partition was incremented systematically and the background distribution was sampled by Monte Carlo under the null hypothesis; the best sensitivity, calculated by the Feldman-Cousins (FC) method [25], is reached at 24% acceptance. The observations in the resulting bins were seven and one events, as shown in Figure 3 (lower). Table 1 confronts observations and background estimates for the partitioned search region.

Reanalysis of FSR data with updated SSR software, motivated by the new L_{eff} measurements of Ref. [22], revealed five events in the FSR search region (which we kept unchanged from the original analysis). Background expectations from SG fitting to these data are also presented in Table 1. In this instance the ^{137}Cs calibration over-predicted the observations very significantly, which we attribute to higher systematic uncertainty in this (FSR) run due to rate-dependent photocathode charging effects [26, 22]. We consider, however, that the SG function provides an appropriate description of our background as validated by the SSR ^{137}Cs calibration. Once the non-negligible neutron contribution is included, the FSR prediction is 7.9±4.8 (cf. 5 observed). The same data-blind optimisation procedure led to a partition at 29%; in this run one event was below that in $\log_{10}$(S2/S1), at 28.8% acceptance.

3.1. Signal inference

A confidence interval for the signal expectation (μ_s) in the SSR acceptance region was obtained with a Profile Likelihood Ratio (PLR) method which accounts for the uncertainty in the background predictions (see, e.g. [27, 28]). We included estimators of the nuisance parameter μ_{b2} from both the SG fits and the ^{137}Cs calibration; the latter is Poisson distributed and the SG predictions are treated as Gaussian truncated at zero. The distribution of profile likelihood ratio was determined by Monte Carlo to ensure correct statistical coverage. The double-sided 90%

CL interval for μ_s was $0 - 5.1$ events. The same procedure applied to FSR data (without a ^{137}Cs prediction in this instance) yielded $0 - 4.2$ events with 90% confidence.

These results are quite robust with respect to the particular choice of binning and test statistic. For example, we conducted two-bin FC calculations with background predictions capped at observation when $\mu_b > n_{obs}$ (so as not to benefit from downward fluctuations of background) and using a 10% acceptance upper bin (as in the original FSR analysis [11]). This yielded the same 4.2 events at 90% CL for the first run and 4.8 for the SSR. These are reassuringly close to the PLR results in Table 1, which treat background uncertainties more formally.

Experimental upper limits on the scalar WIMP-nucleon elastic cross section are shown in Figure 4, calculated with the standard galactic halo model (ρ_o=0.3 GeV/c^2/cm^3, v_o=220 km/s, v_{esc}=544 km/s, and v_E=232 km/s) and the Helm form factor [29] parametrised in Ref. [30]. A minimum cross-section limit of 8.4×10^{-8} pb (90% CL, double sided) is reached at 55 GeV/c^2 WIMP mass for the FSR (similar to the original result [11] and slightly lower than the result reported in Ref. [22] from a single-sided 'maximum patch' test statistic [31]). The minimum of the SSR curve is 4.8×10^{-8} pb, reached at 51 GeV/c^2. The combined result for the ZEPLIN-III experiment, obtained from a four-bin PLR calculation which returns μ_s<6.0 events for the aggregate exposure, is also shown in the figure; the curve minimum is 3.9×10^{-8} pb at 52 GeV/c^2.

Excellent sensitivity to spin-dependent WIMP-neutron interactions is afforded by the odd-neutron isotopes ^{129}Xe and ^{131}Xe. The spin-dependent result is calculated as described in Ref. [12], accounting for the composition of our xenon (depleted in ^{136}Xe) and using Bonn-CD nucleon-nucleon potentials. The FSR+SSR combined curve, shown in Figure 5, has a minimum of 8.0×10^{-3} pb at 50 GeV/c^2 mass. At the time of writing there is no corresponding result from XENON100; this is expected to be a few times lower. The original XENON10 result [32] is not shown in the figure since this had assumed a constant scintillation efficiency and the more favourable ($\sim$2) Bonn A potential; a fair comparison would raise this result to above the ZEPLIN-III curve.
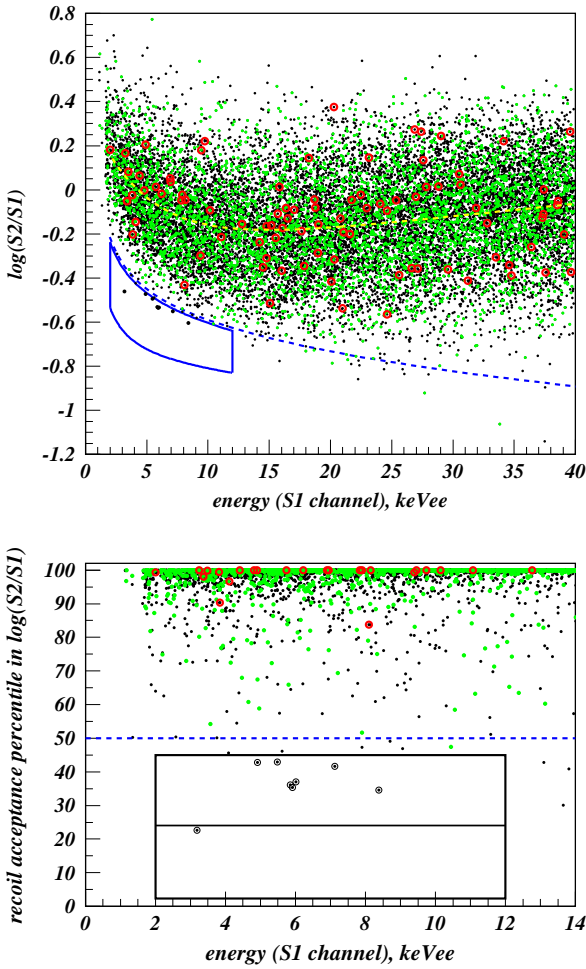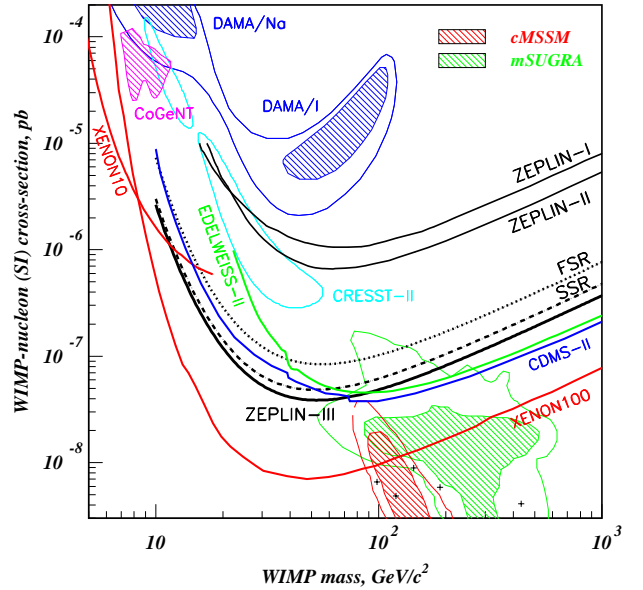
Figure 4: 90%-CL limits on WIMP-nucleon spin-independent cross sections from ZEPLIN-III (FSR, SSR and combined) and from XENON100 [33], XENON10 (low energy analysis [34]), CDMS-II [35] and EDELWEISS-II [36]. Previous results from the ZEPLIN programme are also indicated [37, 38]. In blue we represent the 3- and 5-σ DAMA/LIBRA contours (2008 data, no ion channelling [39]) interpreted in Ref. [40]. The magenta contour is the fit to CoGeNT data under the light WIMP hypothesis [41]; in cyan is the 2-σ region from CRESST-II [42]. The crosses are the original SUSY benchmark points [43]. Favoured regions of parameter space from a 2008 Bayesian analysis in mSUGRA [44] and the likelihood analysis of LHC data within cMSSM [3] are also shown.

Figure 3: Above: fiducial events in full SSR exposure. Green markers label prompt veto coincidences (mostly γ-rays); events in the delayed window (mostly accidental coincidences) are in red. There are 8 unvetoed events in the WIMP acceptance region. The dashed lines show the nuclear and electron recoil band medians (in blue and yellow, respectively). Below: Distribution in signal acceptance (recoils from WIMPs and neutrons are distributed uniformly in the y-axis). There were seven (one) events in the upper (lower) region.

4. Conclusion

In this article we presented experimental upper limits on WIMP-nucleon elastic scattering cross sections from the second run of ZEPLIN-III at Boulby. These were derived from analysis of 1,344 kg·days of fiducial exposure acquired between June 2010 and May 2011. A 90% CL upper limit on the signal content from this exposure allows the exclusion of a scalar WIMP scattering cross section above 4.8×10^{-8} pb/nucleon near 50 GeV/c^2 mass. The combined result for the two runs constrains the scalar cross section to 3.9×10^{-8} pb and the WIMP-neutron spin-dependent cross section to 8.0×10^{-3} pb. Along with XENON100 [33], XENON10 [34], CDMS-II [35] and EDELWEISS-II [36] these results disfavour an interpretation of DAMA in terms of nuclear recoils from WIMPs as

well as recent results from CRESST-II under the canonical dark halo [42]. Models favoured by CoGeNT [41] are harder to rule out completely from our data.

This second run followed the upgrade of the experiment with a new array of purpose-developed, low-radioactivity PMTs, a veto detector based on Gd-loaded polypropylene and plastic scintillator, and new calibration hardware. The automation of the system enabled a 319-day run with excellent stability and reduced manpower underground.

The new photomultipliers were a critical item to reach the design sensitivity of 1×10^{-8} pb·year. Although their radiological background was excellent (35–50 mBq/PMT), their performance compromised the experimental sensitivity by a factor of ~ 4 (from reduction in fiducial mass, of signal acceptance fraction, of cut efficiency and from poorer discrimination). Electron-recoil leakage to below the nuclear recoil median had been 7,800:1 in the FSR compared to only 280:1 in the SSR; no other significant changes were made to the internal hardware.

The addition of a new veto detector proved very valuable, confirming negligible neutron background and providing a useful unbiased sample of γ-ray background for open analysis. In our experience, high-efficiency veto systems will be extremely important in future experiments,
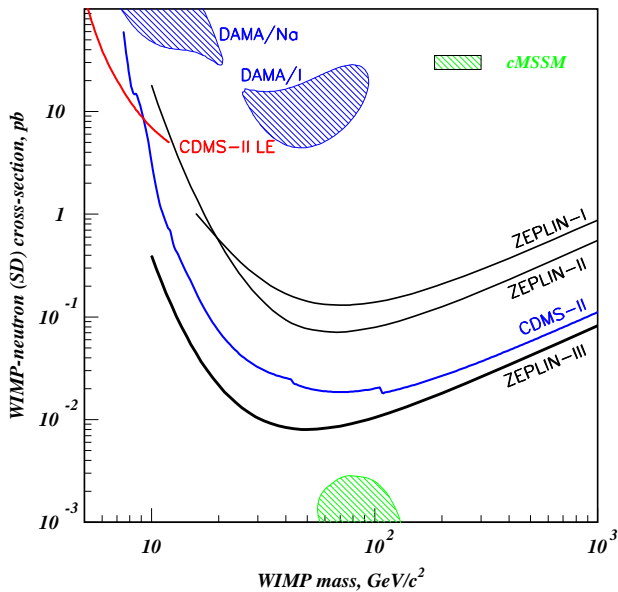
Figure 5: Limits on spin-dependent WIMP-neutron cross section (assuming no proton interaction) from ZEPLIN-III (FSR+SSR, with Bonn CD potentials [45]) as well as CDMS-II (2004-09 data [46, 35] plus low-energy (LE) analysis [47]), ZEPLIN-I [37] and ZEPLIN-II [48]. Also shown is the 3-σ DAMA evidence region (2008 data, no ion channelling [39]) interpreted in Ref. [40]. The green hatched area is the tip of the 95% probability region for cMSSM neutralinos [49].

from the point of view of background reduction, diagnostics and enhancing their discovery power [17].

ZEPLIN-III concludes a successful series of three different LXe-based experiments operated at Boulby since the mid 1990s, with progressively stronger electric fields applied to their active targets. ZEPLIN-I exploited pulse shape discrimination at zero field and produced world-leading results [37]. Delivering 1 kV/cm to the liquid target, ZEPLIN-II was the first two-phase xenon WIMP detector in the world [38, 48]. ZEPLIN-III operated at nearly 4 kV/cm in the first run and achieved the best discrimination of any xenon detector, along with competitive WIMP results in general. As several systems are now being designed and constructed around the world with tonne-scale fiducial masses, the ZEPLIN programme can claim to have pioneered some of the techniques that helped two-phase xenon become a leading technology in the race to discover WIMPs.

5. Acknowledgements

References

[1] ATLAS Collaboration, arXiv:1109.6606v1.
[2] CMS Collaboration, arXiv:1109.2352v1.
[3] O. Buchmueller, et al., Eur. Phys. J. C 71 (2011) 1634.
[4] O. Buchmueller, et al., Eur. Phys. J. C 71 (2011) 1722.
[5] O. Buchmueller, et al., arXiv:hep-ph/1110.3568v1.
[6] D. Y. Akimov, et al., Astropart. Phys. 27 (2007) 46.
[7] H. M. Araújo, et al., Astropart. Phys. 26 (2006) 140.
[8] B. A. Dolgoshein, V. N. Lebedenko, B. U. Rodionov, JETP Lett. 11 (1970) 351.
[9] A. Barabash, A. Bolozdynya, JETP Lett. 49 (1989) 356.
[10] A. Bolozdynya, et al., IEEE Trans. Nuc. Sci. 42 (1995) 565.
[11] V. N. Lebedenko, et al., Phys. Rev. D 80 (2009) 052010.
[12] V. N. Lebedenko, et al., Phys. Rev. Lett. 103 (2009) 151302.
[13] D. Y. Akimov, et al., Phys. Lett. B 692 (2010) 180.
[14] ETEL, http://www.et-enterprises.com.
[15] H. M. Araújo, et al., arXiv:1104.3538.
[16] D. Y. Akimov, et al., Astropart. Phys. 34 (2010) 151.
[17] C. Ghag, et al., Astropart. Phys. 35 (2) (2011) 76.
[18] E. Santos, et al., arXiv:1110.3056v1 [physics:ins-det].
[19] F. Neves, et al., arXiv:1106.0808.
[20] V. Solovov, et al., in preparation.
[21] Tech. Rep. N887, National Physics Laboratory (UK) (2009).
[22] M. Horn, et al., Phys. Lett. B (in press); arXiv:1106.0694.
[23] A. Manzur, et al., Phys. Rev. C 81 (2010) 25808.
[24] G. Plante, et al., arXiv:1104.2587.
[25] G. Feldman, R. Cousins, Phys. Rev. D 57 (7) (1998) 3873.
[26] H. M. Araújo, et al., Nucl. Instrum. Meth. A 521 (2004) 407.
[27] B. Sen, M. Walker, M. Woodroofe, Statist. Sinica 19 (2011) 201.
[28] W. Rolke, A. López, J. Conrad, Nucl. Instrum. Meth. A 551 (2005) 493.
[29] R. H. Helm, Phys.Rev. 104 (1956) 1466.
[30] J. D. Lewin, P. F. Smith, Astropart. Phys. 6 (2006) 87.
[31] S. Henderson, J. Monroe, P. Fisher, Phys. Rev. D 78 (2008) 015020.
[32] J. Angle, et al., Phys. Rev. Lett. 100 (2008) 021303.
[33] E. Aprile, et al., Phys. Rev. Lett. 107 (2011) 131302.
[34] J. Angle, et al., Phys. Rev. Lett. 107 (2011) 051301.
[35] Z. Ahmed, et al., Science 327 (2010) 1619.
[36] E. Armengaud, et al., Phys. Lett. B 702 (2011) 329.
[37] G. J. Alner, et al., Phys. Lett. B 616 (2005) 17.
[38] G. J. Alner, et al., Astropart. Phys. 28 (2007) 287.
[39] R. Barnabei, et al., Eur. Phys. J. C 56 (2008) 333.
[40] C. Savage, et al., JCAP 09 036.
[41] C. Aalseth, et al., Phys. Rev. Lett. 106 (2011) 131301.
[42] G. Angloher, et al., arXiv:astro-ph/1109.0702v1.
[43] J. Ellis, et al., Eur. Phys. J. C 24 (2002) 311.
[44] R. Trotta, et al., JHEP 12 024.
[45] P. Toivanen, et al., Phys. Lett. B 666 (2008) 1.
[46] Z. Ahmed, et al., Phys. Rev. Lett. 102 (2009) 011301.
[47] Z. Ahmed, et al., Phys. Rev. Lett. 106 (2011) 131302.
[48] G. J. Alner, et al., Phys. Lett. B 653 (2007) 161.
[49] L. Roszkowski, R. R. de Austri, R. Trotta, J. High Energy Phys. 07 (2007) 075.